Control of Defects in Deep Drawing of Tailor-welded Blanks for Complex Shape Automotive Panel

Hui Wang (wangxiuhui0412@163.com)
Chongqing Three Gorges University

Lizi Liu
Chongqing Engineering Technology Research Center for Light Alloy and Processing, Chongqing Three Gorges University, Chongqing 404130, China

Haibao Wang
Chongqing Engineering Technology Research Center for Light Alloy and Processing, Chongqing Three Gorges University, Chongqing 404130, China

Jie Zhou
College of Materials Science and Engineering, Chongqing University, Chongqing 400044, China

Research Article

Keywords: Defect, Tailor-welded blanks, Finite element method, Taguchi method, Optimization

Posted Date: February 16th, 2021

DOI: https://doi.org/10.21203/rs.3.rs-230410/v1

Version of Record: A version of this preprint was published at The International Journal of Advanced Manufacturing Technology on January 6th, 2022. See the published version at https://doi.org/10.1007/s00170-021-08406-3.

Control of defects in deep drawing of tailor-welded blanks for complex shape automotive panel

Hui Wang[1,2] · **Lizi Liu**[1,2] · **Haibao Wang**[1,2] · **Jie Zhou**[3]

Abstract

With the development of lightweight vehicles, tailor welded blanks (TWBs) are increasingly used in the automotive industry. Splitting and wrinkling are the main defects during the deep drawing of TWBs. A new method to control the forming defects was introduced in the forming process of TWBs in this study. The microstructure and mechanical properties of TWBs were characterized through metallography and tensile tests. Finite element modelling of an automobile rear door inner panel made of TWBs was built to analyse deep drawing. Edge cutting and notch cut were introduced in the drawing to deal with forming defects and reduce the number of stamping tools. The minimum distance between the material draw-in and trimming lines, thinning index and thickening index were defined as the measurable index to analyse the numerical results. Orthogonal experiment, numerical simulation and multiobjective experiment were utilised to optimize the forming parameters. The proposed method and optimised parameters were verified through experiments. The experimental results are basically consistent with the numerical simulation. Results demonstrate that the proposed method can provide some guidance for controlling the defects in deep drawing of TWBs for complex shape automotive panel.

Keywords

Defect · Tailor-welded blanks · Finite element method · Taguchi method · Optimization

✉ Hui Wang
wangxiuhui0412@163.com

[1] College of Mechanical Engineering, Chongqing Three Gorges University, Chongqing 404130, China
[2] Chongqing Engineering Technology Research Center for Light Alloy and Processing, Chongqing Three Gorges University, Chongqing 404130, China
[3] College of Materials Science and Engineering, Chongqing University, Chongqing 400044, China

1. Introduction

With the development of industrial technology, an increasing number of families have acquired private cars, causing heavy pressure to transportation and environment [1]. Therefore, energy saving and environmental protection attract increasing attention from the public.

In recent years, lightweight automobiles made of lightweight materials haves become the development trend, because they can save energy and reduce carbon emission [2]. The forming of Tailor-welded blanks (TWBs) is a valid method used to actualize automotive lightweight [3]. TWBs are welded from several different plates with different thickness, mechanical properties and surface coatings [4]. The use of TWBs forming technique has many advantages in the automotive industry [5, 6]. They can reduce the number of parts and stamping tools. In addition, they can enhance the safety performance of vehicles and reduce vehicle weight at the same time [7].

The advantage of the stamping forming of TWBs is different mechanical properties can be obtained at different areas of the part by using the blank with different materials or thickness [8]. Compared with the conventional stamping process, the stamping forming of TWBs can effectively reduce the number of tools, welding work and assembly costs [9].

Studies of the TWBs have been a hot topic in recent years [10]. Overall, the existing reports on TWBs mainly concentrated on themicrostructure, mechanical properties, formability, forming limit diagram, failure, residual stresses, forming and applications of these materials [11-14]. Mechanical properties of TWBs rest with many factors, such as material, welding method, weld line orientation and thickness ratio of the blanks [15, 16]. The uniaxial tensile test is widely used to research the mechanical properties of TWBs. Zadpoor et al. [17] utilized the monaxial tension test to obtain the mechanical properties of TWBs. Ciubotariu et al. [18] investigate the behavior and mechanical properties of the weld line in a TWBs during and after its tensile testing by using parallel tensile tests, micro-hardness tests, thermography, EDX, and microscopy. Xu et al. [19] studied the mechanical properties of TWBs with different weld line orientations by three-point bending tests. Song et al. [5] studied the influences of the thickness ratio of the base materials on the formability of TWBs. Miles et al. [20] found the welding method will affect the formability of TWBs. Rossini et al. [21] researched the mechanical properties, microstructure and failure modes of TWBs with dissimilar materials utilizing

metallography, microhardness, and tensile tests. Liu et al. [22] investigated the deformation behavior and failure features of TWBs in hot forming.

Challenges have increased in the development of stamping tools by increasing part complexity and usage of TWBs to reduce the weight of a vehicle [23]. Accurate forming simulations are the driving force during the engineering phase. Accurate simulation can reduce the cost of tools manufacturing and reject rates of parts [24]. Several studies have found that the numerical simulation is an effective tool for analyzing the stamping forming process of TWBs [25-27]. The finite element (FE) modelling of TWBs is more complex than that of the single material plate because of the existence of the weld [28].

Two approaches are developed to deal with the weld seam for the numerical simulation of TWBs in practice [8]. The first approach is to consider the geometry and property of the weld seam in the FE modelling. The second approach is to simplify or ignore the weld seam in the FE modelling when it has higher strength than that of the base materials. In this case, failure is more likely to occur in the base materials than in the weld seam. Determining the better method depends on the types, geometry and mechanical properties of the base metal and the weld seam. Raymond et al. [29] introduced FE modelling of TWBs using solid elements, including weld properties and geometry. Buste et al. [30] considered the weld seam of TWBs as rigid links in the FE modelling. However, few investigations have been done on the defects control in deep drawing of TWBs.

This paper aimed to study the deep drawing of TWBs for complex shape automotive panel. A typical rear door inner panel was studied as a case in the research. The microstructure and mechanical properties of the base material and TWBs were characterised through metallography and tensile tests to achieve accurate FE modelling. Edge cutting and notch cut were introduced in the drawing process to deal with the forming defects and reduce the number of tools. Orthogonal experiment, numerical simulation and multiobjective experiment were utilised to optimise the forming parameters. The proposed method and optimised parameters were verified through experiments.

2. Materials

2.1 Microstructure

As shown in Fig. 1, an automobile rear door inner panel made of TWBs was researched in this article. The blanks of this part were welded by two plates which the thickness were 0.7 mm and 1.2 mm, respectively. Considering the self-weight and assembly position of the part, the area close to B-pillar and hinge needs high strength and stiffness. Thus, the thickness of the part close to B-pillar and hinge was thicker than that close to C-pillar. This feature can enhance the strength and stiffness of the automobile rear door inner panel whilst maintaining its weight.

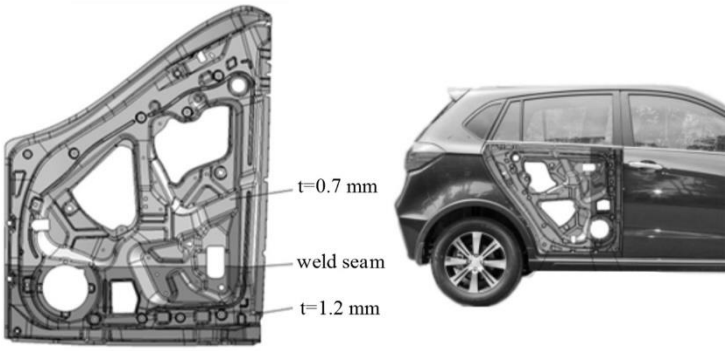

Fig. 1 Automobile rear door inner panel

The base material of the TWBs used for this part is DC05 and belongs to cold-rolled low carbon steel for deep drawing. The chemical composition of DC05 is presented in Table 1. As shown in Fig. 2, the microstructure of TWBs was determined through metallographic microscopy. The cross-section of the welded joint is illustrated in Fig. 2a. The microstructure of the base material was mainly composed of ferrite (Fig. 2b). The heat-affected zone (HAZ) was made up primarily of bainite and ferrite (Fig. 2c), and the weld zone was made up primarily of bainite (Fig. 2d). The microstructure of the base materials, HAZ and weld seam were different. As shown in Fig. 3, the fracture surfaces of the base material and weld seam were characterised through TESCAN VEGA3 LMH scanning electron microscopy (SEM) after tensile tests. As shown in Fig. 3a, the fracture surface of the base material is numerous isometric dimples, which is ductile dimple fracture pattern. In addition, the fracture morphology of the weld seam made up of a great deal of river pattern and cleavage facets, which is typical ductile and cleavage fractures.

Table 1 Chemical composition of DC05 (wt.%)

C	Mn	P	S	Alt	Fe
≤0.008	≤0.3	≤0.02	≤0.02	≤0.015	balance

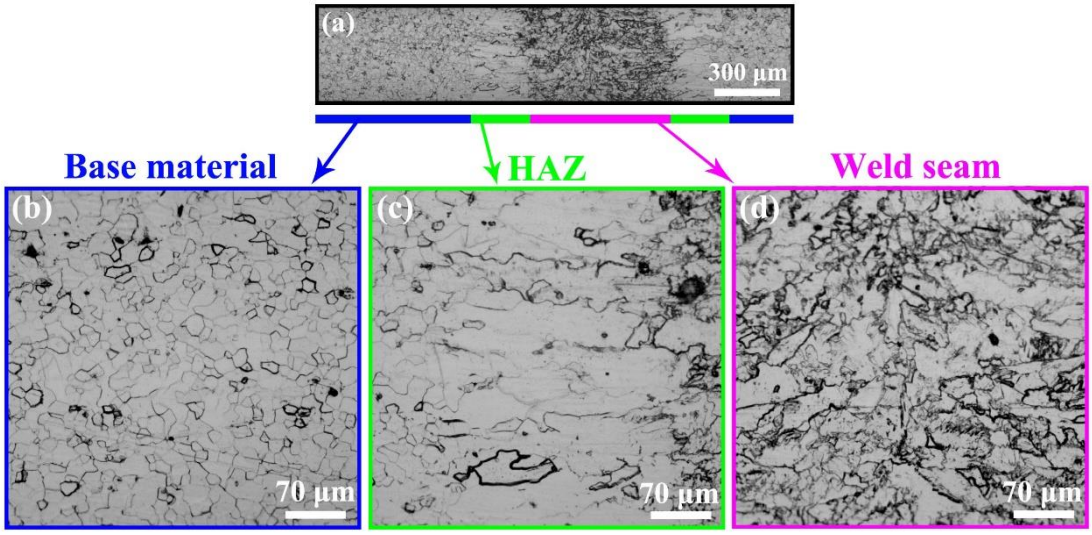

Fig. 2 Microstructures of the TWBs: (a) welded joint, (b) base material, (c) HAZ, and (d) weld seam

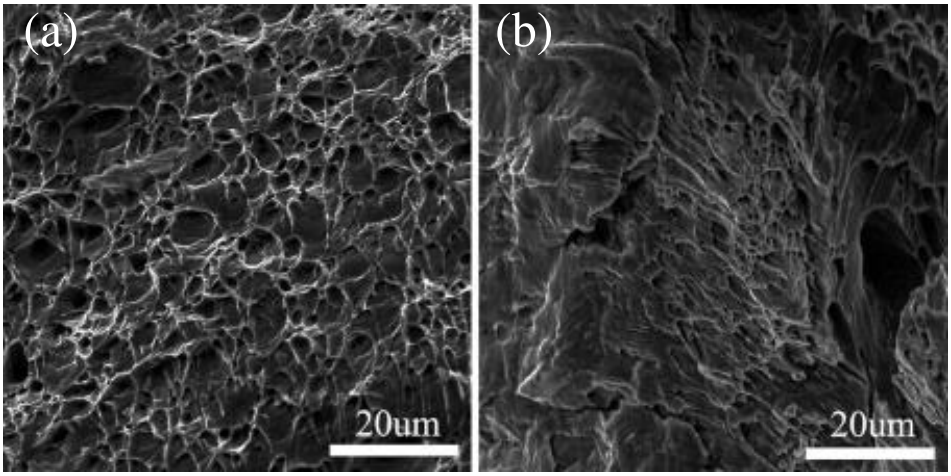

Fig. 3 Fracture morphology of the TWBs: (a) base material, and (b) weld seam

2.2 Mechanical properties

Accurate numerical simulation is based on reasonable material model and FE modelling. Tensile tests were performed before the numerical simulation to determine the yield strength, tensile strength and flow curves of the base materials and the TWBs. According to ASTM-E8 standard test [31], the flow curve described the strain-stress relationship of the base materials of the TWBs were studied on a universal testing machine at room temperature. The tensile specimen of the TWBs based on Ref 32 as well as engineering stress–strain curves are illustrated in Fig. 4. The flow curves of the thick sheet and thin sheet are similar, however the flow curves of the base material are quite different from that of the TWBs on the basis of tensile

tests. The yield stress and tensile strength of the TWBs are higher than that of the base materials. The yield stress of the TWBs is 325.16 MPa, whereas that of thick sheet and thin sheet are 123.84 and 129.87 MPa, respectively. The tensile strength of the TWBs is 339.09 MPa, whereas that of thick sheet and thin sheet are 281.70 and 276.86 MPa, respectively. The elongation to failure of the TWBs is lower than that of the base materials. The elongation to failure of the TWBs is 11.07%, whereas that of thick sheet and thin sheet are 54.84% and 55.75%, respectively.

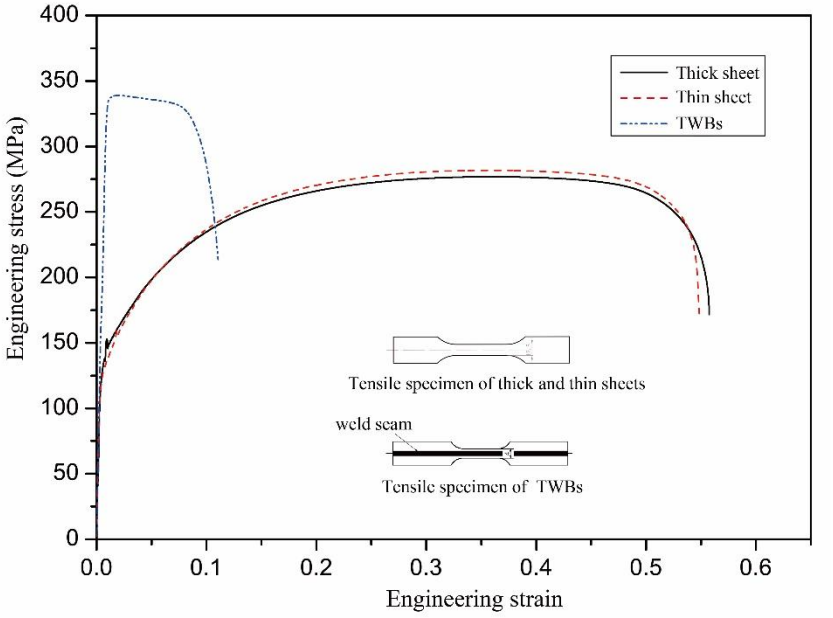

Fig. 4 Engineering stress–strain curves

3. FE models

Automotive rear doors consist of left and right doors, and they are symmetrical in shape. Considering the uniqueness of automobile rear door inner panels, they are usually formed in a large tool simultaneously, which is called two-cavity in one tool. Based on the structure analysis of the automobile rear door inner panel, the forming process of the automobile rear door inner panel includes drawing, trimming, piercing, reshaping and separating. The first step, drawing, is performed to form the part shape, followed by trimming and piercing operations and a final step that is needed to reshape and separate the left and right door inner panels. The design of die addendum and binder surfaces of the automobile rear door inner panel is illustrated in Fig. 5. The forming defect of the similar automobile panel usually occurs during drawing. Thus, the investigation of defect control for this part focuses on the drawing stage. Numerical simulation

is a useful tool to predict various forming defects in the development of stamping tools [33, 34].

Fig. 5 Design of die addendum and binder surfaces of the part

As shown in Fig. 6, the FE modelling of the drawing processes of the automobile rear door inner panel was built to analyse the drawing process using the FE software Autoform. The FE modelling consists of die, blank, binder and punch. The size and form of the initial blank were determined on the basis of the desired final part geometry, die addendum and binder surfaces. The initial blank was set as a triangular element with a size of 1800 mm×1270 mm and thickness of 0.7 and 1.2 mm. The weld seam was taken as the rigid links in the finite element modelling because the weld area is extremely narrow and the strength and hardness of the weld seam are larger than that of the base materials in laser welding [30].

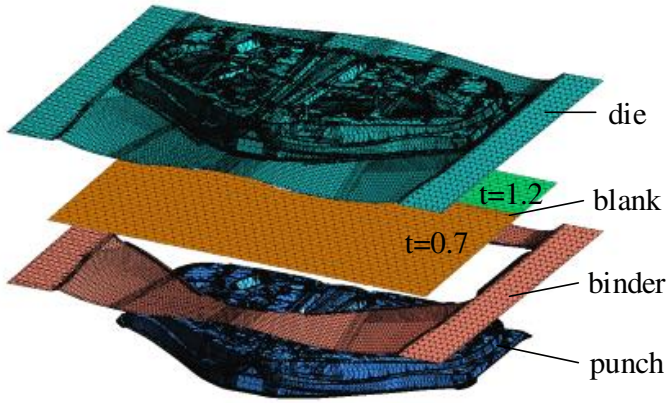

Fig. 6 FE modelling of the drawing processes of the automobile rear door inner panel

The die, binder and punch were taken as rigid bodies during the drawing process. The drawing of TWBs was divided into three steps, namely, the gravity loading stages, closing of blank holder stages and drawing stages. The elastic shell element was defined in the gravity

loading stage, and the elastic plastic shell element was defined in the closing of blank holder stages and drawing stages. The stress–strain curves of the material was based on tensile tests. The material model used in the FE modelling was Banabic-Balan-Comsa (BBC) yield function, and material parameters were referred to the method used in Ref 35. Lubrication conditions are taken into account for the friction in the simulation. A coulomb model with stick slip modeling was used in the FE models. The friction coefficient applied is assumed between all tools and blank. A constant friction coefficient, μ=0.125, was defined in the simulation [36]. The velocity of the upper tooling (die) was 1 mm/s in the forming process in the FE models [8].

4. Improvement of process design

The preliminary FE analysis of the part was conducted on the FE software. Since the part is symmetrical, the half of the part on one side of the symmetry line can show the full result. The formability diagram of the formed part is shown in Fig. 7. As shown in Fig. 7, few defects, such as splitting and wrinkling, were found on the formed part. These defects were caused by many reasons, such as uneven material draw-in, material thinning and complex shape. For similar problems, Ouyang [37] proposed a secondary drawing process to improve the defects. However, this method increases the drawing process time and leads to a long part production cycle.

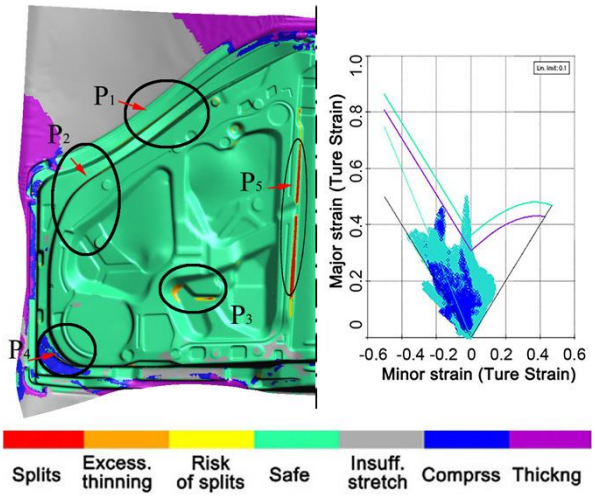

Fig. 7 Formability diagram of numerical simulation at the end of drawing

To deal with the forming defects, such as splitting and wrinkling, in the initial results of numerical simulation, combined with the trimming line and piercing position of the final

product of the part, the improvement of the process design for the automobile rear door inner panel was conducted as follows:

(1) Edge cutting was introduced at the beginning of the drawing process to cut the excess material of the blank. As shown in Figs. 7 and 8, edge cutting, K_{1a} was introduced to cut the excess material of the sheet for avoiding the splitting in the area of P_1. Compared with traditional process, blanking was integrated in the drawing die.

(2) Considering the characteristics of large irregular holes on the part, notch cut was introduced to solve the splitting defects near irregular holes during the drawing process. As shown in Figs. 7 and 8, notch cuts, K_{2a} was introduced to avoid the splitting in the area of P_2 and P_3. Notch cuts, K_{3a} was introduced to fix the splitting in the area of P_3 and P_4. Notch cut, K_4, was introduced to avoid the splitting in the area of P_5.

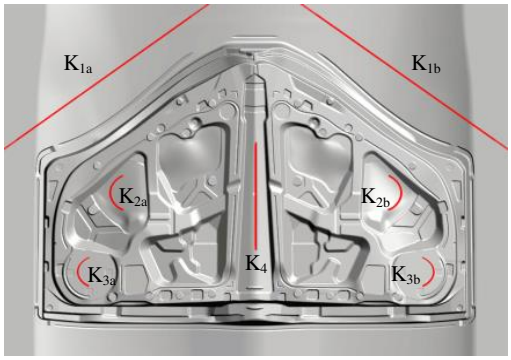

Fig. 8 Distribution of the edge-cutting and the notch cut introduced in the drawing process

The cut-in time of edge cutting and notch cut is closely related to the forming quality of the part. The material boundary line will flow into the trimming line or the piercing line when the cut-in time of edge cutting and notch cut is extremely early. Splitting and wrinkling may occur on the formed part when the cut-in time of edge cutting and notch cut is extremely late. The cut-in time is extremely crucial in obtaining the qualified parts. Thus, the cut-in time of edge cutting and notch cut needs to be accurately controlled.

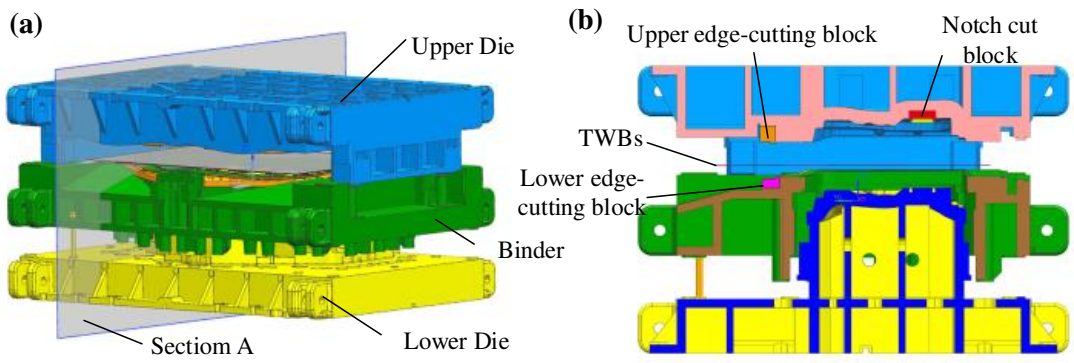

Fig. 9 Drawing tools: (a) three-dimensional models; (b) view of section A

The drawing process of the automobile rear door inner panel consists of the gravity loading stages, closing of blank holder stages and drawing stages. The main deformation, edge cutting and notch cut occurred in the drawing stage. The cut-in time of edge cutting and notch cut was defined as the displacement of the upper die. The displacement was set to 0 mm when the upper die come into contact with the blank at the beginning of blank holder closing stage. The total displacement of the upper die was 151.2 mm when the upper and lower dies fully matched (Fig. 10).

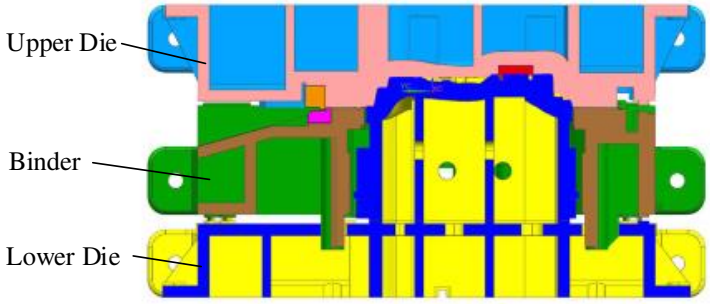

Fig.10 The upper and lower dies fully matched (the displacement of the upper die was 151.2 mm)

5. Results and discussion

5.1 Orthogonal design and results

Taguchi method is a powerful and commonly used technique for the design of experiments [38, 39]. Xu et al. [39] investigated the discrete optimisation design of TWB thin-walled structures using the Taguchi method. Thus, to achieve the best results of the cut-in time of edge cutting and notch cut, orthogonal experimental design and numerical simulation were used to optimise the deep drawing of TWBs. In the orthogonal experiment, the edge cutting of K_{1a} and K_{1b} were defined as experimental factors A, the notch cut of K_{2a} and K_{2b} was defined as

experimental factors B, the notch cuts of K_{3a} and K_{3b} were defined as experimental factors C, the notch cut of K_4 was defined as experimental factors D, and the blank-holder force (BHF) was defined as experimental factors E. To determine the optimal parameter combination, the experiments with five four-level factors were established using the orthogonal experimental design. The range of those factors was determined through a single-factor experiment. As presented in Table 2, the orthogonal array table can be expressed as L_{16} (4^5).

Table 2 Design of orthogonal experiment

Levels	A	B	C	D	E
	K_1(mm)	K_2(mm)	K_3(mm)	K_4(mm)	F (10^4 N)
1	0	130	130	140	90
2	10	135	135	142	100
3	20	140	140	144	110
4	30	145	145	146	120

On the basis of the established orthogonal experiment with five four-level factors, 16 experimental groups with different factors and levels can be obtained, as shown in Table 3. The simulation was conducted using the FE software. The edge cutting and notch cut were defined as open cutting that can separate the meshes of the blank along an open line in the FE software, and the cut-in times of A, B, C and D depended on the displacement of the upper die.

The minimum distance between the material draw-in line and trimming line (L), thinning index (T_1), and thickening index (T_2) were recorded and taken as the optimisation objectives. The calculation formulas of L, T_1, and T_2 were defined as follows:

$$L = Min\{L_{K1} \ , \ L_{K2} \ , \ L_{K3} \ , \ L_{K4}\} \tag{1}$$

$$T_1 = \frac{S_t}{S_0} \times 100\% \qquad t \geq 25\% \tag{2}$$

$$T_2 = \frac{S_t}{S_0} \times 100\% \qquad t \leq -5\% \tag{3}$$

L_{Ki} is the minimum distance between the material draw-in and trimming lines in notch cut K_i. t is the thinning rate. S_t refers to the area of the part that meets the requirement of the thinning rate. S_0 is the total area of the part.

The minimum distance between the material draw-in and trimming lines can be measured by showing the trimming and piercing lines in the post processing of the software. The thinning

and thickening indices are calculated by highlighting the area where the thinning rate is more than 25% and the thinning rate is less than −5% in different colours. The results are summarised in Table 3.

Table 3 Results of orthogonal design

No.	A	B	C	D	E	*L(mm)*	T_1(%)	T_2(%)
1	1	1	1	1	1	1.31	0.200	0.830
2	1	2	2	2	2	3.92	0.197	0.886
3	1	3	3	3	3	7.67	0.192	0.866
4	1	4	4	4	4	11.39	0.220	0.792
5	2	1	2	3	4	6.43	0.162	0.783
6	2	2	1	4	3	1.79	0.148	0.857
7	2	3	4	1	2	1.31	0.204	0.805
8	2	4	3	2	1	4.06	0.234	0.785
9	3	1	3	4	2	8.14	0.144	0.850
10	3	2	4	3	1	7.48	0.159	0.753
11	3	3	1	2	4	1.92	0.189	0.695
12	3	4	2	1	3	1.49	0.252	0.817
13	4	1	4	2	3	4.08	0.169	0.827
14	4	2	3	1	4	1.39	0.190	0.789
15	4	3	2	4	1	6.48	0.158	0.769
16	4	4	1	3	2	2.01	0.235	0.776

Extreme difference analysis was introduced to determine the effect of those factors on the minimum distance between the material draw-in and trimming lines, thinning index and thickening index. The result of extreme difference analysis is presented in Table 4. *R* is the range fluctuation index of each factor. The magnitude of the value of R is proportional to the magnitude of the factor influence. Extreme difference analysis results show that notch cut K_4 (D) is the biggest influence factor influencing the minimum distance between the material draw-in and trimming lines, notch cuts, K_{2a} and $K_{2b,}$ (B) were the most important factor influencing the thinning index, and BHF (E) was the most important factor influencing the thickening index.

Table 4 Results of extreme difference analysis

		A	B	C	D	E
L	R	2.689	1.360	4.323	5.560	1.540
	Rank	3	5	2	1	4
T_1	R	0.016	0.066	0.005	0.044	0.007
	Rank	3	1	4	2	5

T_2	R	0.064	0.039	0.034	0.023	0.077
	Rank	2	3	4	5	1

5.2 Multiobjective optimisation

The multiobjective experiment was introduced to determine the optimal combination of the cut-in time of edge cutting, notch cut and BHF. The established multiobjective function and constraint equation is shown in function 4. The optimisation objective of L was defined as the maximum objective function, and the optimisation objective of T_1 and T_2 was defined as the minimum objective function. The limit inferior for L was 5 mm.

$$\begin{cases} Max \quad L \\ Min \quad T_1 \\ Min \quad T_2 \end{cases}$$
$$s.t. \quad T_1 = \frac{S_{t_1}}{S_0} \times 100\% \qquad t_1 \geq 25\% \tag{4}$$
$$T_2 = \frac{S_{t_2}}{S_0} \times 100\% \qquad t_2 \leq -5\%$$
$$L \geq 5$$

The experimental design software Design-Expert was used to calculate the multiobjective optimisation results under the constraints of multiobjective equations. The results are presented in Table 5. Five group results that satisfy the multiobjective function are list in Table 5. The first solution has the highest desirability value and is determined as the optimal parameter combination. The optimal parameter combination obtained by multiobjective optimisation is A=20 mm, B=140 mm, C=145 mm, D=146 mm, and E=120×10^4 N.

Table 5 Results of multi-objective optimization

No.	A	B	C	D	E	*L(mm)*	*T_1(%)*	*T_2(%)*	Desirability
1	20	140	145	146	120	9.68	0.154	0.718	0.655
2	20	140	130	146	120	5.37	0.159	0.713	0.646
3	20	140	145	144	120	8.63	0.173	0.696	0.622
4	30	140	145	146	120	8.41	0.156	0.730	0.610
5	20	140	145	146	90	9.23	0.151	0.738	0.601

As shown in Figs. 11 and 12, the optimal result was verified using the FE software. The forming limit diagram of the part after optimisation is shown in Fig. 11 and the thinning distribution diagram of the part after optimisation is shown in Fig. 12 in drawing,. The forming

limit diagram clearly shows that the optimised part was fully formed, the safe area covered most of the area of the drawing part, and the wrinkling area of the part was outside the trimming line.

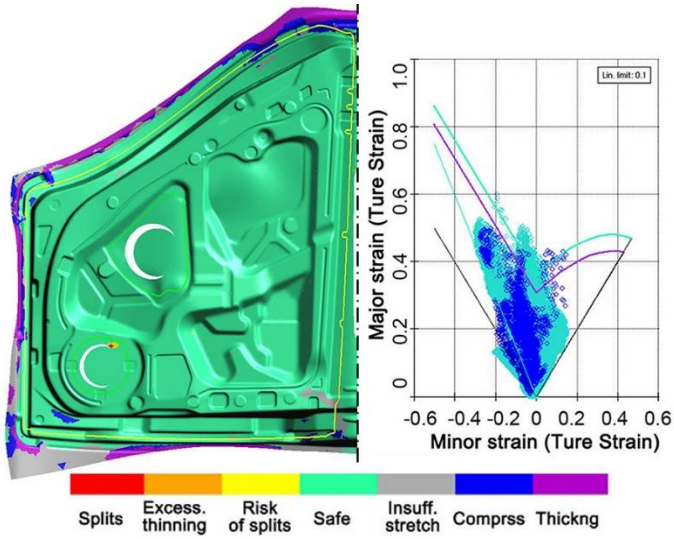

Fig. 11 Forming limit diagram of the part at the end of the drawing after optimization

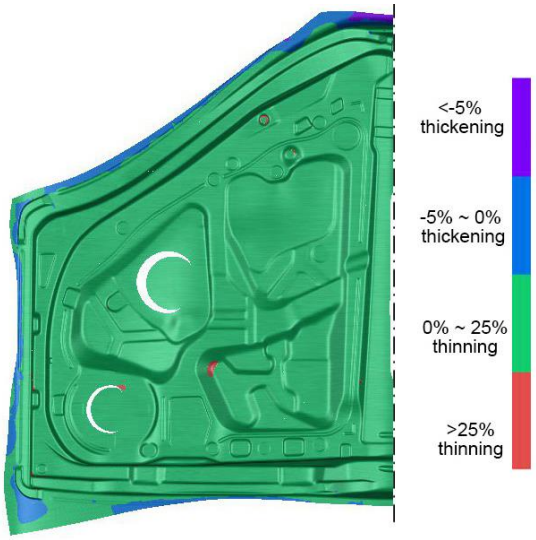

Fig. 12 Thinning distribution diagram of the part after optimization

5.3 Experimental verification

The drawing tools used in the experiment are shown in Fig. 13. The die tryout was conducted in a single-action sheet metal stamping hydraulic press using the optimised parameter combination. The cut-in time of edge cutting and notch cut was controlled and realised by adjusting the position of the edge cutting and notch cut blocks in the tools in assembly. The tryout sheet of TWBs is made from DC05 with a size of 1800 mm×1270 mm

and thickness of 0.7 and 1.2 mm. As shown in Fig. 14, the appearance of tryout parts and numerical simulation results are very close. The tryout part is fully formed from the appearance inspection. The tryout part has minimal wrinkling in the area of the binder surface and does not affect the final product because this area is outside the trimming line and will be cut in the subsequent process. The thicknesses of the final product area were measured by a micrometre. The minimum thickness of the thick sheet area of the formed part is 0.950 mm, and that of thin sheet area of the formed part is 0.528 mm. The thinning rate of thicknesses can meets the requirement of thickness tolerance of the part. The forming defect on the automobile rear door inner panel was controlled because of the introduction of edge cutting and notch cut and the best cut-in time. The numerical simulation results agree with the experimental results. Thus, the proposed method can provide guidance to actual production.

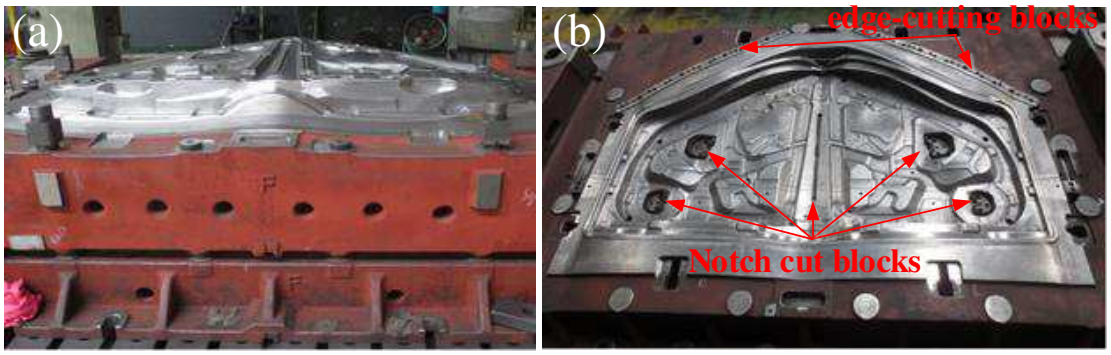

Fig. 13 Drawing tools in the experiment: (a) Lower die and binder; (b) Upper die

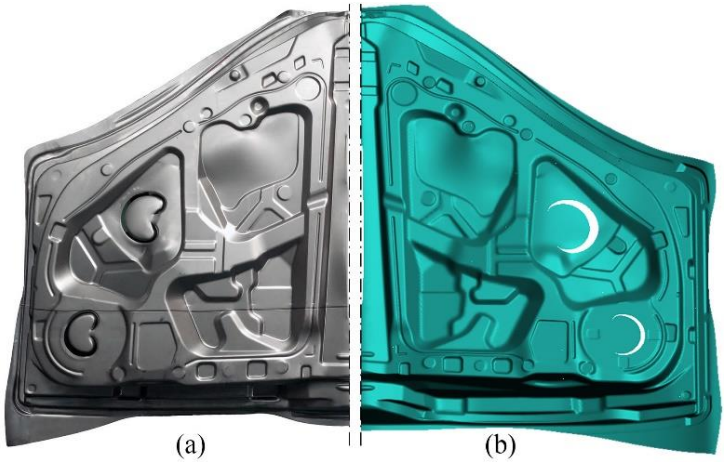

Fig. 14 (a) Tryout part in the experiment; (b) the drawing part of the simulation

6. Conclusions

1) The microstructure of the different regions of TWBs were different, which is the main

factor that causes the difference in the mechanical properties of the base materials and TWBs. The tensile strength, yield strength and elongation to failure of the thin and thick materials are similar. The yield and tensile strengths of the TWBs are larger than that of the base materials, and the elongation to failure of the TWBs is lower than that of the base materials.

2) The cut-in time of edge cutting and notch cut was investigated in this study. Splitting and wrinkling may occur on the formed part when the cut-in time of edge cutting and notch cut is extremely late. The material boundary line will flow into the trimming line or the piercing line when the cut-in time of edge cutting and notch cut is extremely early.
3) The minimum distance between the material draw-in and trimming lines, thinning index and thickening index were defined as the measurable indices to analyse the numerical results, making it extremely convenient for the statistical results and subsequent optimisation analysis.
4) The orthogonal and multiobjective experiments are valuable tools for analysing and optimising multiple process parameters. The optimal parameter combination was verified through experiments. Numerical simulation and experimental results indicate that the proposed method is feasible to deal with the forming defects and reduce the number of tools and can guide actual production.

Ethics declarations

The authors declare that they have no known competing financial interests or personal relationships that could have appeared to influence the work reported in this paper.

Consent to participate

The authors declares that they consent to participate this paper.

Consent to Publish

This manuscript is approved by all authors for publication.

Authors Contributions

H. Wang designed the study, performed the research, analysed data, and wrote the paper. LZ.

Liu has carried out the mechanics experiment and microscopic characterization. HB. Wang and J. Zhou has revised the manuscript.

Funding

This research was supported by the Science and Technology Research Program of Chongqing Municipal Education Commission (No. KJQN201801228), Chongqing Natural Science Foundation (No. CSTC2019JCYJ-MSXM1349) and by Chongqing Engineering Research Center Funds for Colleges (No. 2019YJZX0101).

Competing Interests

The authors declare no competing interests.

Availability of data and materials

The authors declare that all date and material support their published claims and comply with field standards.

References

1. Wu T, Shen Q, Xu M, Peng T, Ou X (2018) Development and application of an energy use and CO2 emissions reduction evaluation model for China's online car hailing services. Energy 154:298-307
2. Kaluza A, Kleemann S, Fröhlich T, Herrmann C, Vietor T (2017) Concurrent Design & Life Cycle Engineering in Automotive Lightweight Component Development. Procedia CIRP 66:16-21
3. Kong H, Chao Q, Rolfe B, Beladi H (2019) One-step quenching and partitioning treatment of a tailor welded blank of boron and TRIP steels for automotive applications. Mater Des. https://doi.org/10.1016/j.matdes.2019.107799
4. Saunders FI, Wagoner RH (1996) Forming of tailor-welded blanks. MMTA 27(9):2605-2616
5. Song Y, Hua L (2014) Influences of Thickness Ratio of Base Sheets on Formability of Tailor Welded Blanks. Procedia Engineering 81:730-735
6. Pallett RJ, Lark RJ (2001) The use of tailored blanks in the manufacture of construction components. J Mater Process Technol 117(1):249-254
7. Kinsey BL (2011) 7 - Tailor welded blanks for the automotive industry. In: Kinsey BL, Wu X (ed) Tailor Welded Blanks for Advanced Manufacturing. Woodhead Publishing, pp 164-180

8. Wang H, Zhou J, Zhao TS, Liu LZ, Liang Q (2016) Multiple-iteration springback compensation of tailor welded blanks during stamping forming process. Mater Des 102:247-254
9. Merklein M, Johannes M, Lechner M, Kuppert A (2014) A review on tailored blanks—Production, applications and evaluation. J Mater Process Technol 214(2):151-164
10. Basak S, Katiyar BS, Orozco-Gonzalez P, Baltazar-Hernandez VH, Arora KS, Panda SK (2019) Microstructure, forming limit diagram, and strain distribution of pre-strained DP-IF steel tailor–welded blank for auto body application. Int J Adv Manuf Technol. https://doi.org/10.1007/s00170-019-03938-1
11. Zadpoor AA, Sinke J (2010) 10 - Weld metal ductility and its influence on formability of tailor welded blanks. In: Sun X (ed) Failure Mechanisms of Advanced Welding Processes. Woodhead Publishing, pp 258-288
12. Schwinn J, Besel M (2019) Determination of residual stresses in tailored welded blanks with thickness transition for crack assessment. Engineering Fracture Mechanics 208:209-220
13. Köklü U (2013) Investigation into the formability of Al-1050 tailor-welded blanks with antilock braking system. Int J Adv Manuf Technol 66(1):221-229
14. Russo Spena P, Cortese L, Nalli F, Májlinger K (2019) Local formability and strength of TWIP-TRIP weldments for stamping tailor welded blanks (TWBs). Int J Adv Manuf Technol 101(1):757-771
15. Abbasi M, Ketabchi M, Ramazani A, Abbasi M, Prahl U (2012) Investigation into the effects of weld zone and geometric discontinuity on the formability reduction of tailor welded blanks. Comp Mater Sci 59:158-164
16. Bandyopadhyay K, Basak S, Panda SK, Saha P (2015) Use of stress based forming limit diagram to predict formability in two-stage forming of tailor welded blanks. Mater Des 67:558-570
17. Zadpoor AA, Sinke J, Benedictus R (2007) Mechanics of tailor welded blanks: An overview. Key Eng Mat 344:373-382
18. Ciubotariu V, Brabie G (2011) Weld line behaviour during uniaxial tensile testing of tailor welded blanks. Arch Civ Mech Eng 11(4):811-824
19. Xu F, Sun G, Li G, Li Q (2014) Experimental investigation on high strength steel (HSS) tailor-welded blanks (TWBs). J Mater Process Technol 214(4):925-935
20. Miles MP, Nelson TW, Decker BJ (2004) Formability and strength of friction-stir-welded aluminum sheets. MMTA 35(11):3461-3468
21. Rossini M, Spena PR, Cortese L, Matteis P, Firrao D (2015) Investigation on dissimilar laser welding of advanced high strength steel sheets for the automotive industry. Mat Sci Eng A-Struct 628:288-296
22. Liu J, Wang A, Gao H, Gandra J, Beamish K, Zhan L, Wang L (2018) Transition of failure mode in hot stamping of AA6082 tailor welded blanks. J Mater Process Technol 257:33-

44
23. Gomes T, Silva FJG, Campilho RDGS (2017) Reducing the Simulation Cost on Dual-phase Steel Stamping Process. Procedia Manufacturing 11:474-481
24. Sigvant M, Pilthammar J, Hol J, Wiebenga JH, Chezan T, Carleer B, den Boogaard Tv (2019) Friction in sheet metal forming: influence of surface roughness and strain rate on sheet metal forming simulation results. Procedia Manufacturing 29:512-519
25. Wang A, Liu J, Gao H, Wang L-L, Masen M (2017) Hot stamping of AA6082 tailor welded blanks: Experiments and knowledge-based cloud – finite element (KBC-FE) simulation. J Mater Process Technol 250:228-238
26. Gautam V, Kumar A (2019) Experimental and Numerical Studies on Formability of Tailor Welded Blanks of High Strength Steel. Procedia Manufacturing 29:472-480
27. Qiu XG, Chen WL (2007) The study on numerical simulation of the laser tailor welded blanks stamping. J Mater Process Technol 187-188:128-131
28. Zadpoor AA, Sinke J, Benedictus R (2011) 4 - Numerical simulation modeling of tailor welded blank forming. In: Tailor Welded Blanks for Advanced Manufacturing. Woodhead Publishing, pp 68-94
29. Raymond SD, Wild PM, Bayley CJ (2004) On modeling of the weld line in finite element analyses of tailor-welded blank forming operations. J Mater Process Technol 147(1):28-37
30. Buste A, Lalbin X, Worswick MJ, Clarke JA, Altshuller B, Finn M, Jain M (2000) Prediction of Strain Distribution in Aluminum Tailor Welded Blanks for Different Welding Techniques. Can Metall Quart 39(4):493-502
31. ASTM E 8M (2003) Standard test methods of tension testing of metallic materials [metric]. In: Annual book of ASTM standards, vol. 3.01. USA: American Society for Testing and Materials
32. Gong H, Wang S, Knysh P, Korkolis YP (2016) Experimental investigation of the mechanical response of laser-welded dissimilar blanks from advanced- and ultra-high-strength steels. Mater Des 90:1115-1123
33. Sun Y, Li Y, Daniel WJT, Meehan PA, Liu Z, Ding S (2017) Longitudinal strain development in Chain-die forming AHSS products: Analytical modelling, finite element analysis and experimental verification. J Mater Process Technol 243:322-334
34. Gronostajski Z, Pater Z, Madej L, Gontarz A, Lisiecki L, Łukaszek-Sołek A, Łuksza J, Mróz S, Muskalski Z, Muzykiewicz W, Pietrzyk M, Śliwa RE, Tomczak J, Wiewiórowska S, Winiarski G, Zasadziński J, Ziółkiewicz S (2019) Recent development trends in metal forming. Arch Civ Mech Eng 19(3):898-941
35. Banabic D, Carleer B, Comsa D-S, Kam E, Krasovskyy A, Mattiasson K, Sester M, Sigvant M, Zhang X (2010) Sheet metal forming processes: Constitutive modelling and numerical simulation. Springer
36. Firat M, Karadeniz E, Yenice M, Kaya M. (2013) Improving the Accuracy of Stamping

Analyses Including Springback Deformations. J Mater Eng Perform 22:332-337
37. Ouyang BY (2012) Numerical simulation of drawing process for laser tailor-welded blank of car door inner plate. Forging & Stamping Technology 37(1):41-44
38. Wen T, Wang H, Yang C, Liu LT (2014) On a reshaping method of clinched joints to reduce the protrusion height. Int J Adv Manuf Technol 71(9):1709-1715
39. Xu F, Zhang S, Wu K, Dong Z (2018) Multi-response optimization design of tailor-welded blank (TWB) thin-walled structures using Taguchi-based gray relational analysis. Thin Wall Struct 131:286-296

Figures

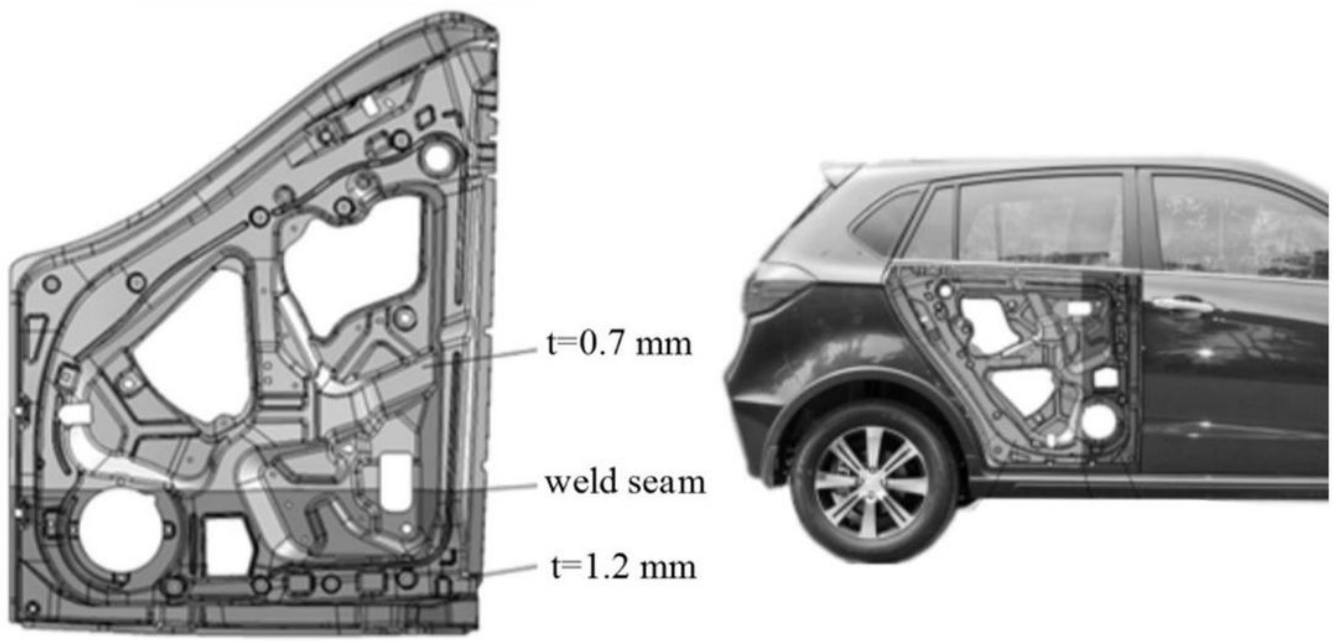

Figure 1

Automobile rear door inner panel

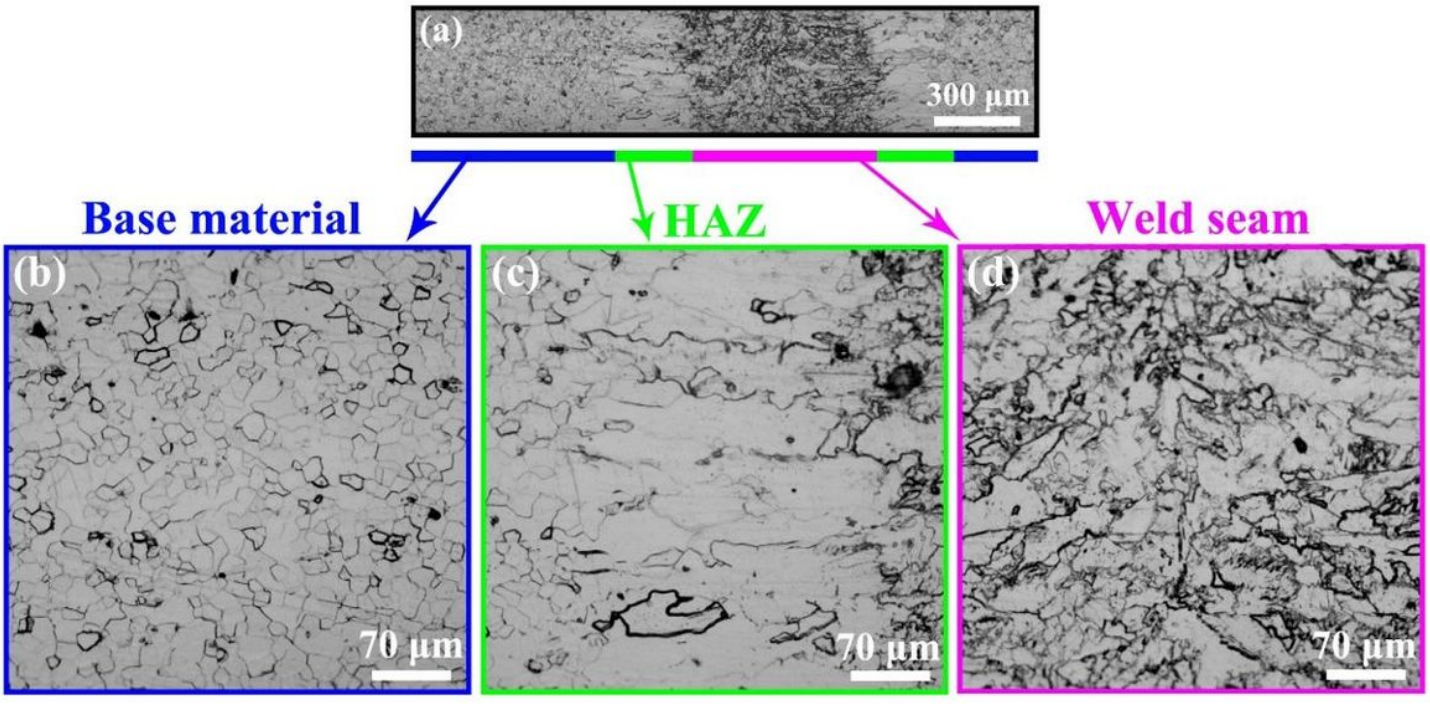

Figure 2

Microstructures of the TWBs: (a) welded joint, (b) base material, (c) HAZ, and (d) weld seam

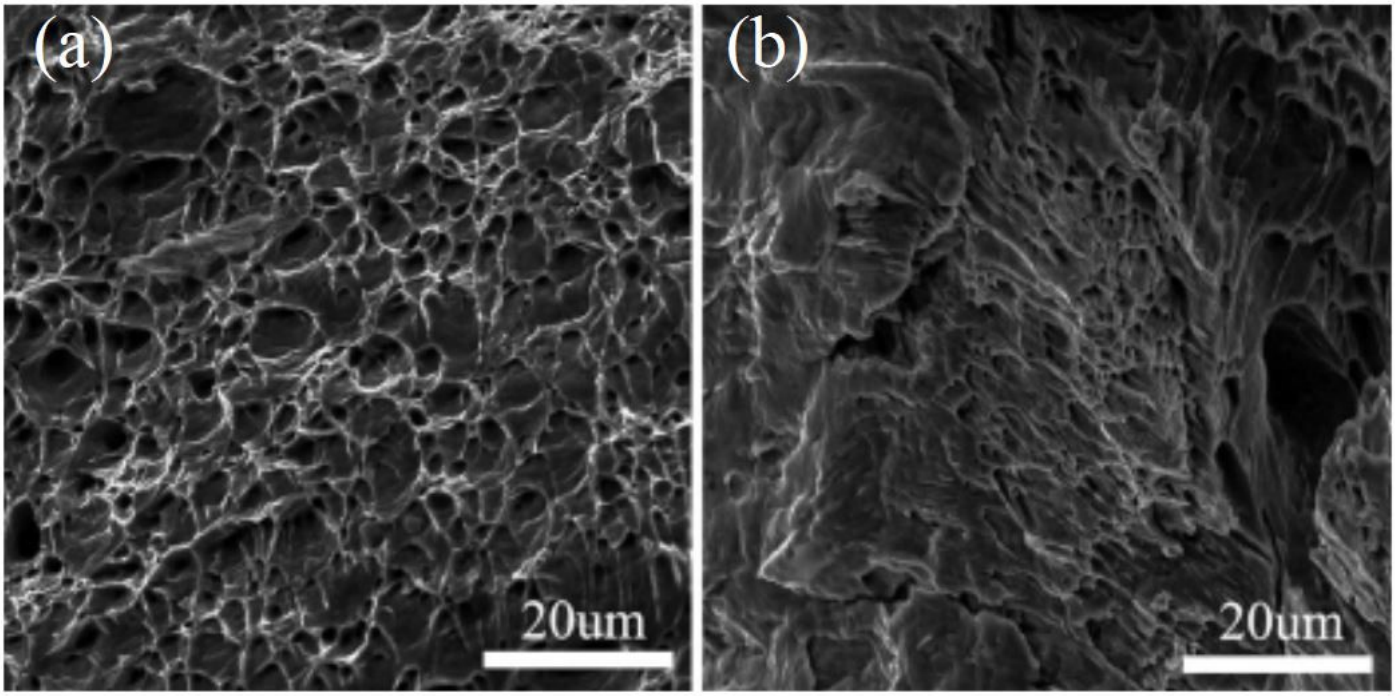

Figure 3

Fracture morphology of the TWBs: (a) base material, and (b) weld seam

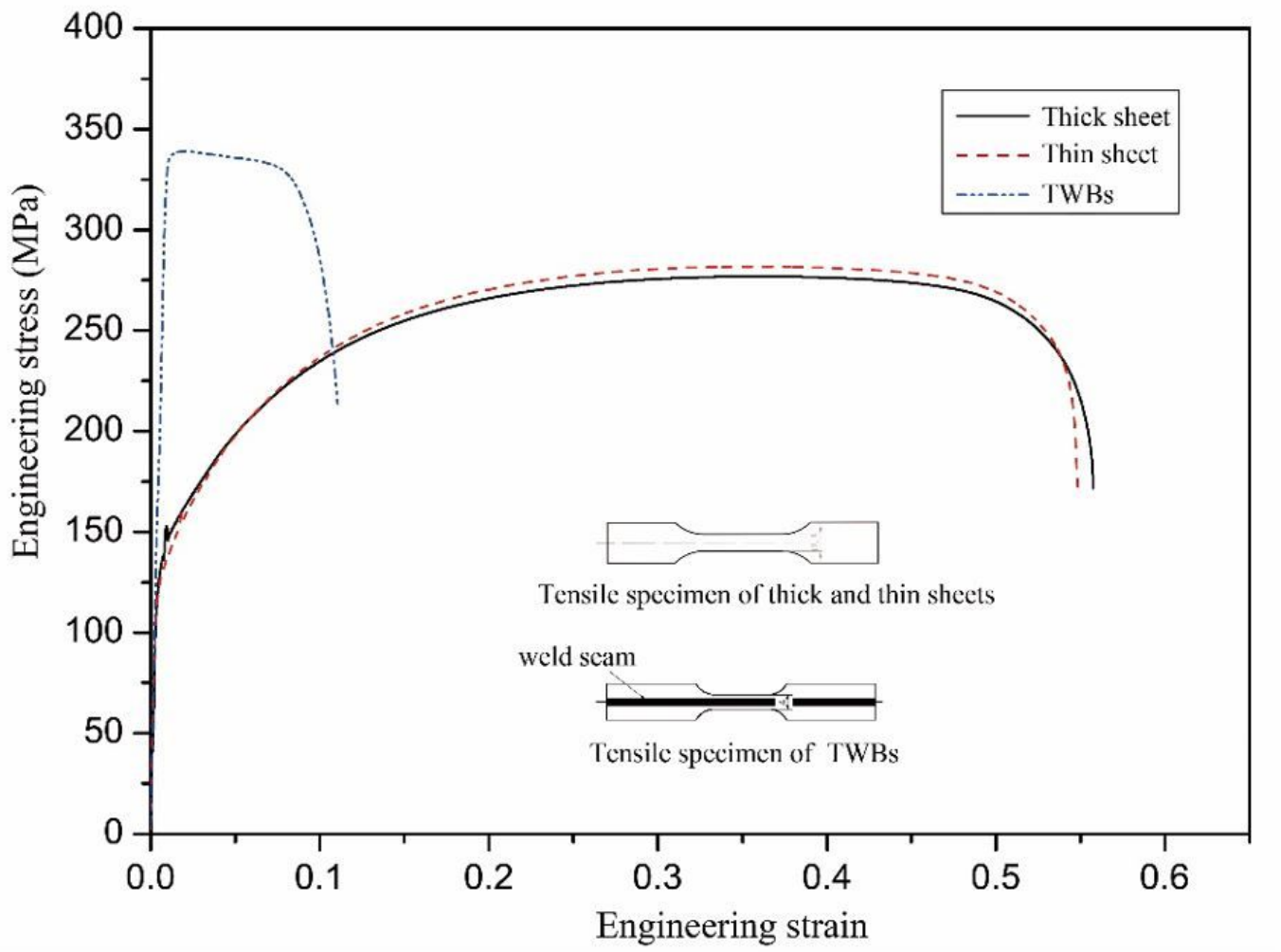

Figure 4

Engineering stress–strain curves

Figure 5

Design of die addendum and binder surfaces of the part

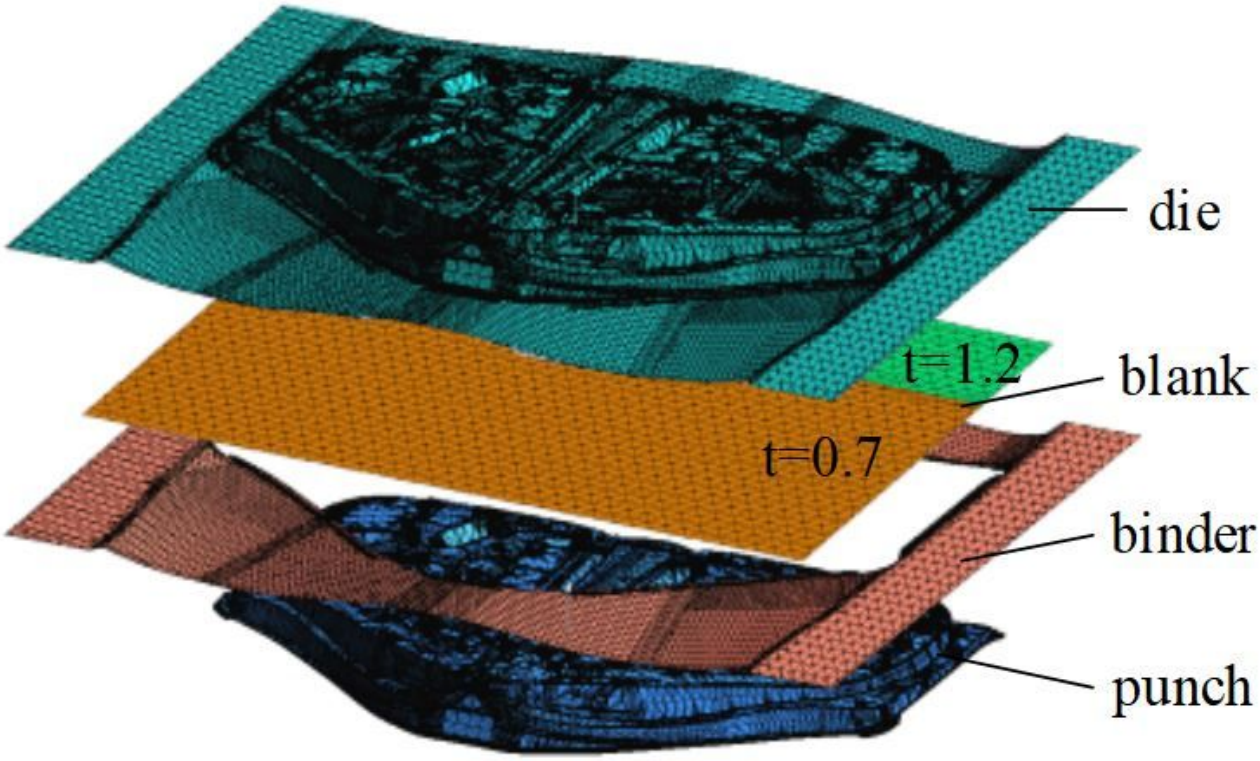

Figure 6

FE modelling of the drawing processes of the automobile rear door inner panel

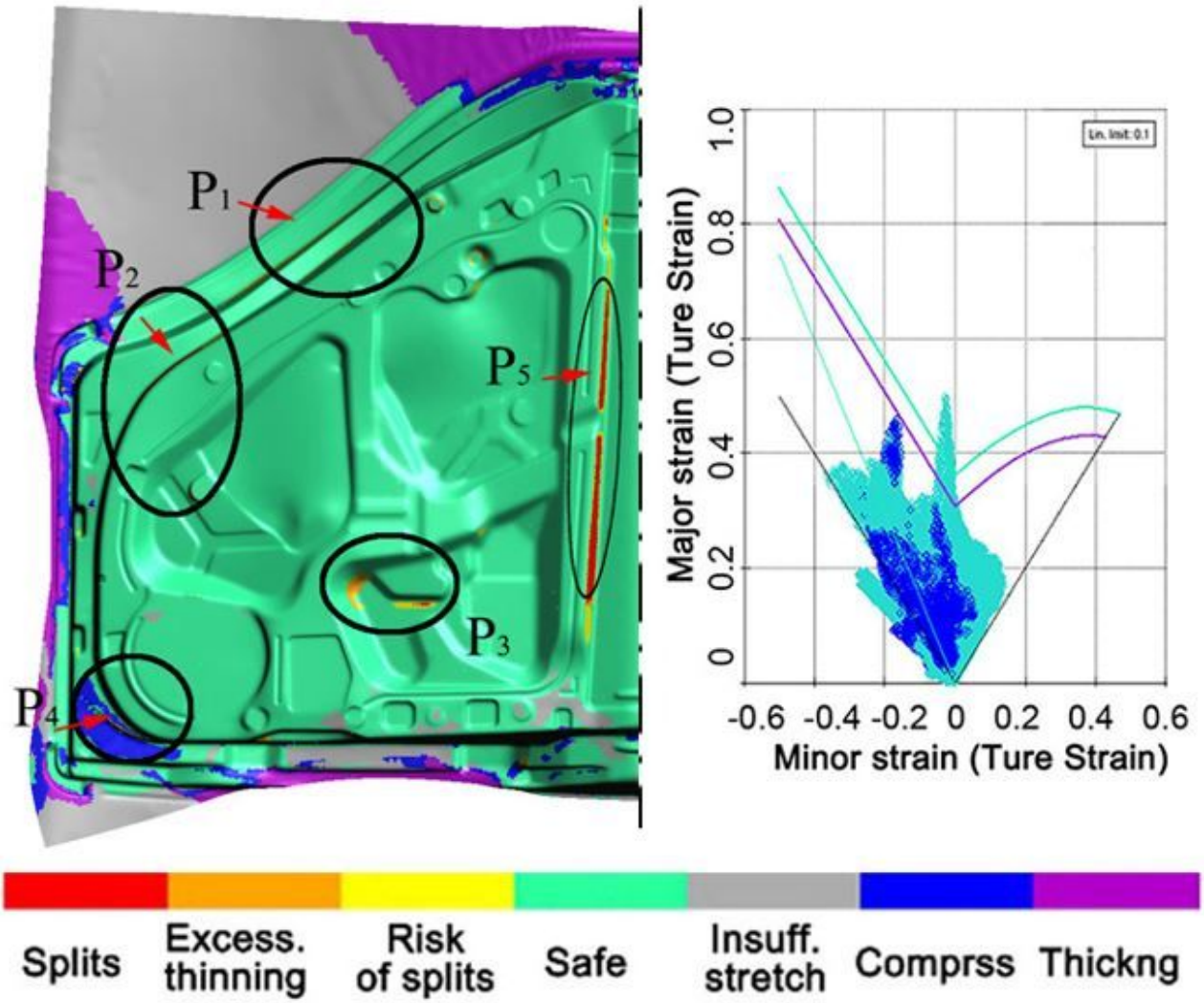

Figure 7

Formability diagram of numerical simulation at the end of drawing

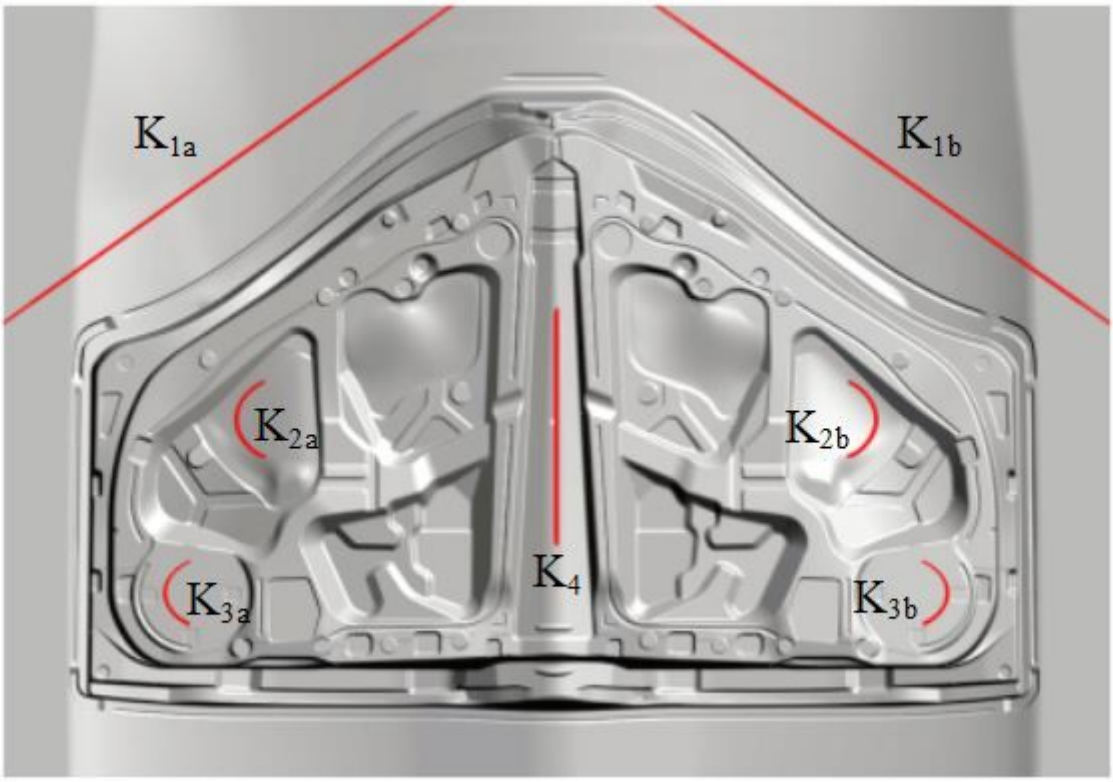

Figure 8

Distribution of the edge-cutting and the notch cut introduced in the drawing process

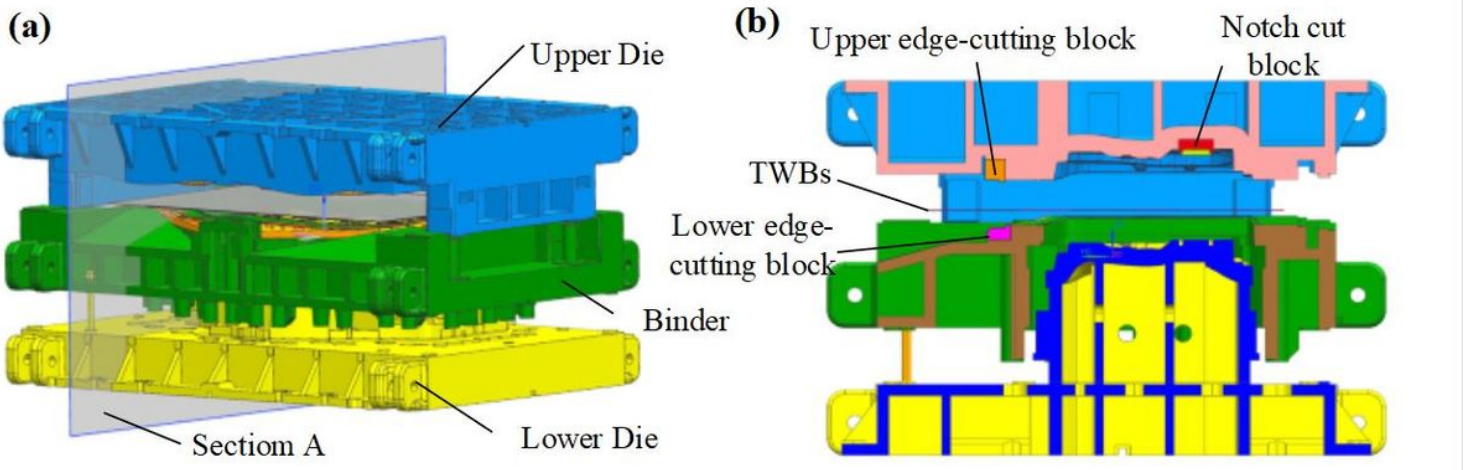

Figure 9

Drawing tools: (a) three-dimensional models; (b) view of section A

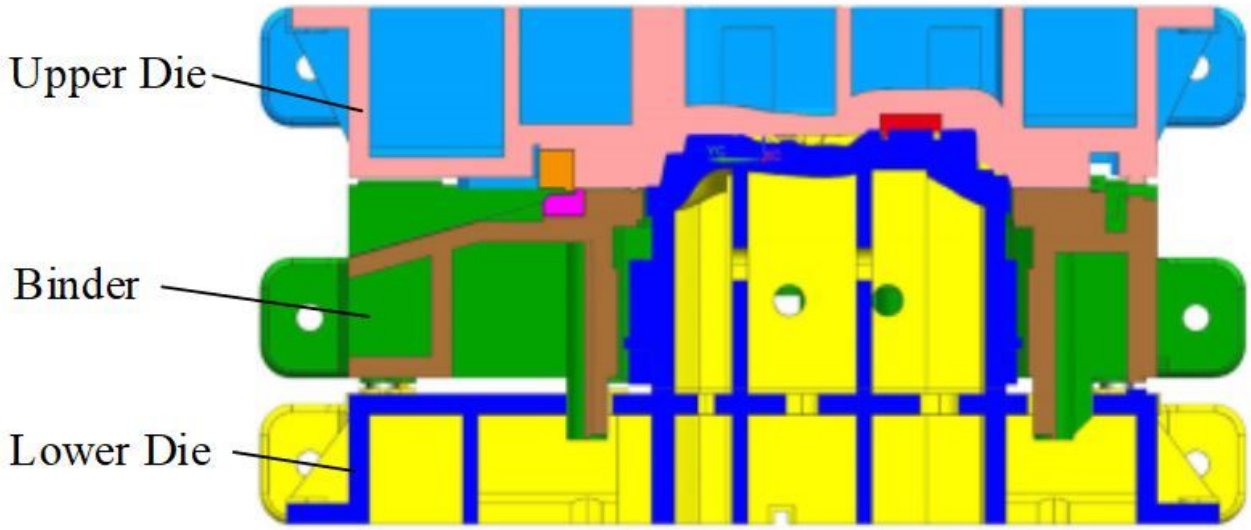

Figure 10

The upper and lower dies fully matched (the displacement of the upper die was 151.2 mm)

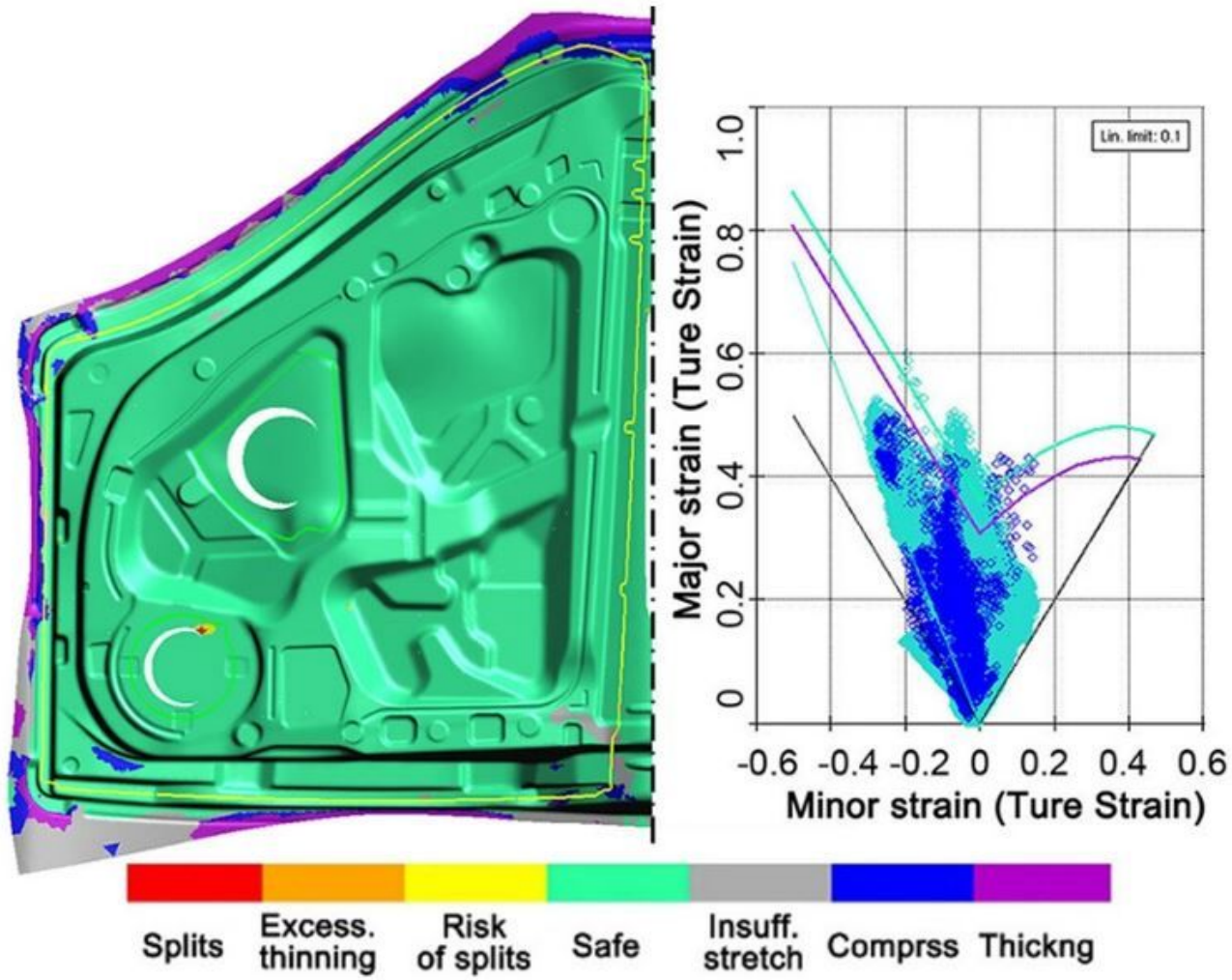

Figure 11

Forming limit diagram of the part at the end of the drawing after optimization

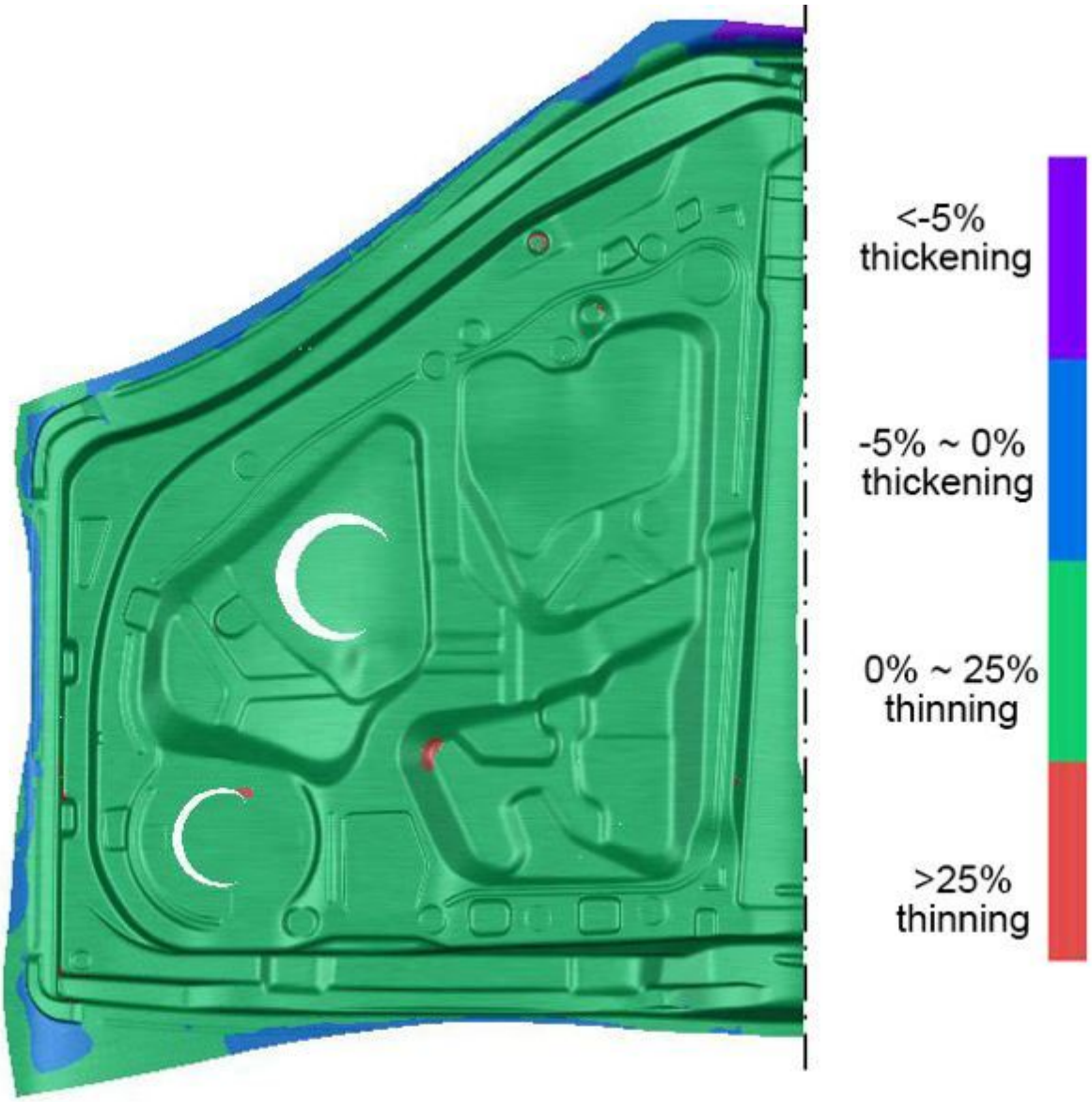

Figure 12

Thinning distribution diagram of the part after optimization

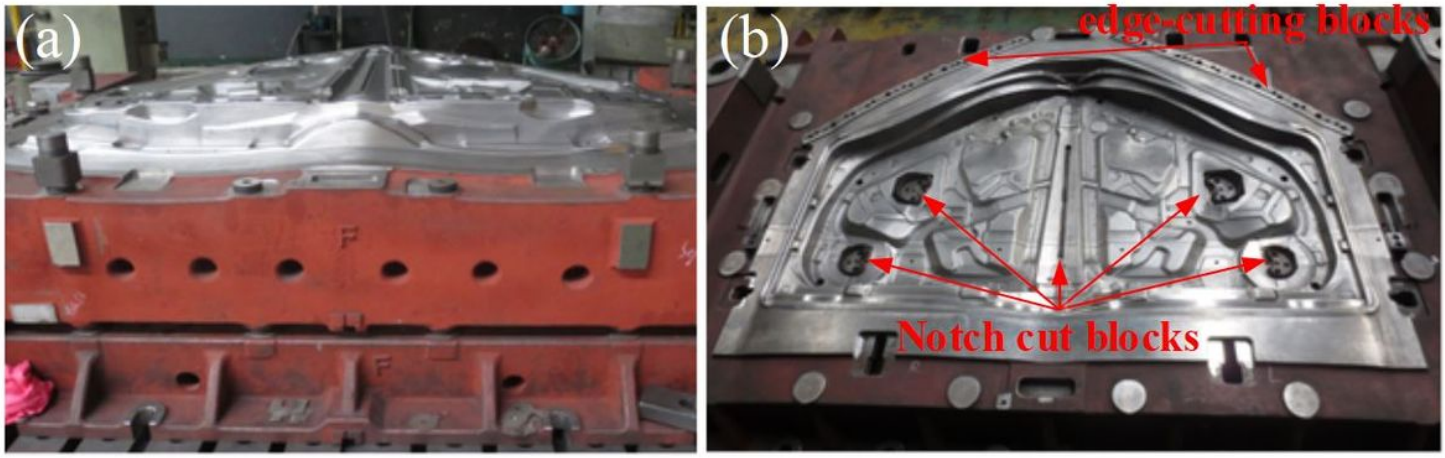

Figure 13

Drawing tools in the experiment: (a) Lower die and binder; (b) Upper die

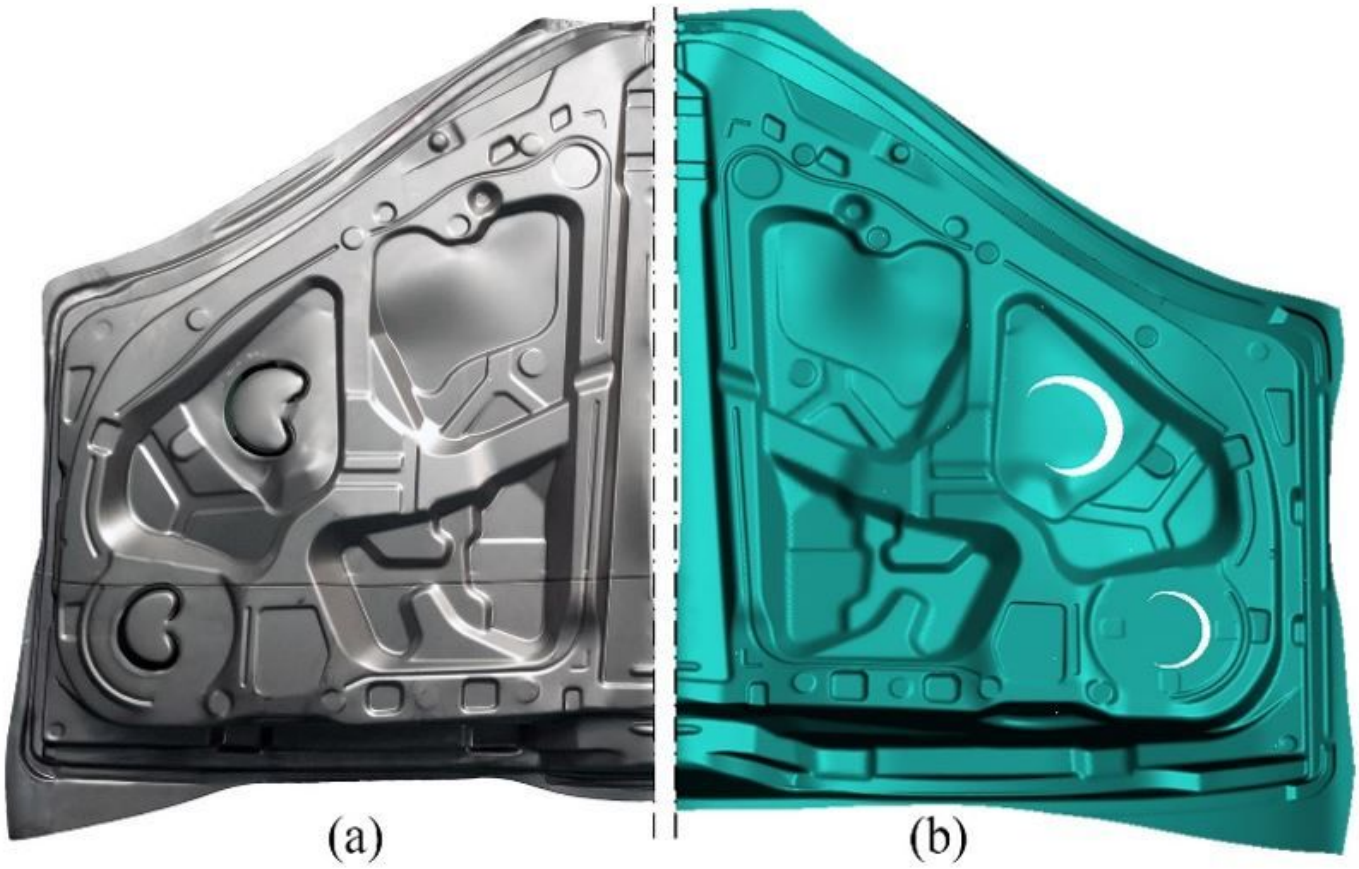

Figure 14

(a) Tryout part in the experiment; (b) the drawing part of the simulation